

Analysis of dielectric and electrical transport properties of NdFeAsO ceramic

G. K. Mishra¹, N. K. Mohanty^{1*}, B. Behera²

¹Centurion University of Technology and Management, School of Applied Science, Department of Physics, Odisha, India

²Sambalpur University, School of Physics, Materials Research Laboratory, Odisha, India

Abstract

The iron-based ceramic NdFeAsO was synthesized by the solid-state reaction method. The tetragonal crystal structure was confirmed at room temperature through the X-ray diffraction technique. The dielectric characteristics i.e. dielectric constant (ϵ_r) and loss tangent ($\tan\delta$) of the sample were studied at a wide range of temperature and frequencies with an impedance analyzer and revealed that these quantities decreased with an increase in frequency. The dielectric anomalies were observed in the studied sample, which was found to be shifting towards the higher temperature side on increasing the frequency. The analysis of ac conductivity data of the compound obeyed Jonscher's universal power law as well as the Arrhenius equation. The compound showed a negative temperature coefficient of resistance (NTCR) behavior. The electrical conduction mechanism in the sample can be explained through the correlated barrier hopping (CBH) model.

Keywords: X-ray diffraction, ceramic materials, dielectric properties, conductivity, density of states.

INTRODUCTION

The iron-based ceramic NdFeAsO is one of the families of layered high-temperature superconductors with a transition temperature of around 50 K. Superconductivity was initially studied in metals such as lead [1], cuprates [2], iron oxypnictides [3], bismuth [4], graphene [5], and even H₂S [6], which undergo transitions to superconducting states under suitable conditions. The discoveries of iron-based superconductors (FeSCs) have been greatly emphasized by the researchers due to the simultaneous existence of their superconductivity and magnetic properties, having a layered structure [7-14]. The Fe-based RFeAsO_{1-x}F_x of rare earth family having R= Sm, Ce, Nd, Pr, Gd, Tb, and Dy compounds come under FeSCs having the highest superconductivity transition temperature ($T_c \sim 54$ K). In these compounds, superconductive properties may be manifested due to FeAs and R(O/F) layers in which the former layer behaves as superconductive planes and the latter layer serves as charge reservoirs [15-17]. Among these, the compound NdFeAsO_{1-x}F_x materials have a layered tetragonal crystal with crystallographic axes $a=b=3.962$ Å and $c=8.555$ Å [18-21]. Also, enhancement of magnetic properties in FeSCs is observed with the change of concentration of O/F [20].

Realizing the importance of layered FeSCs particularly its superconducting nature at low temperature we have planned to synthesize the iron-based polycrystalline ceramic compound and to study its structural, dielectric, and electrical properties at high temperature in order to have a complete

systematic study of the said compound over a large range of temperature. Part of the theory may be developed in order to understand the conduction mechanism in the sample. Further, this study may provide the scope for use of these materials in two different applications such as to control the loss of energy through superconducting materials and store the energy through dielectric materials.

EXPERIMENTAL

The ceramic material NdFeAsO was prepared by solid-state reaction technique, which is a common synthesis method dealing with high temperature to obtain polycrystalline material from solid reagents [21]. The pure oxides Nd₂O₃ (99.99%, Spectrochem, India), Fe₂O₃ ($\geq 99\%$, Loba Chem., India), and As₂O₃ ($\geq 95\%$, Spectrochem, India) were taken in a suitable stoichiometric proportion. The stoichiometrically weighed compounds were mixed thoroughly in air atmosphere for 2 h and then in methanol for 2 h by using an agate mortar and pestle to get a homogeneous mixture of the materials. The mixed powders were calcined at 1100 °C for 5 h in a high purity alumina crucible with cover in order to control the evaporation of the components in an air atmosphere. The process of grinding and calcination was repeated several times till the formation of the compound was confirmed. The quality and formation of the calcined compounds were checked through an X-ray diffraction (XRD) method at room temperature through a powder diffractometer (Ultima IV, Rigaku, Japan) using CuK α radiation ($\lambda=1.5405$ Å) in a wide range of Bragg's angle 2θ ($20^\circ \leq 2\theta \leq 80^\circ$) with a scanning rate of 3 °/min. The calcined powder was mixed with polyvinyl alcohol (PVA), which was used as a binder to reduce the brittleness of the pellets

*nilayaphy@gmail.com

 <https://orcid.org/0000-0003-4120-2875>

and generally burns off during the sintering process. The fine homogenous powder was cold-pressed into cylindrical pellets of 10-12 mm diameter and 1-2 mm of thickness at a pressure of 3.5×10^6 N/m² using a hydraulic press. The pellet was then sintered at 1150 °C for 6 h. After sintering, in order to have both faces flat and parallel, the pellet was then polished with fine emery paper. For carrying out any electrical measurement, the flat polished surfaces of the pellet were then coated with an air-drying conducting silver paste. The pellet was dried at 150 °C for 2 h to remove the moisture (if any) and cooled to room temperature before taking any electrical measurements. The frequency and temperature dependence dielectric properties of the compound were measured using an LCR meter (mod. 3532, Hioki, Japan) in the frequency range of 10^2 - 10^6 Hz from 25 to 450 °C. For the measurement of dielectric properties with temperature, the samples were kept in a vertical fit furnace through a sample holder. The vertical fit furnace was connected with a variac for heating purposes. The temperature was recorded by a thermocouple (chromel-alumel) connected with a dc micro voltmeter with an accuracy of 0.01 mV (equivalent to an accuracy in temperature of ± 0.25 K).

RESULTS AND DISCUSSION

Structural analysis: the room temperature XRD profile of NdFeAsO is shown in Fig. 1. Based on the earlier work, we have refined the XRD data of the prepared sample with a tetragonal crystal system and most of the peaks were well matched with the previous report [22]. There was a good agreement between observed and calculated values of interplanar spacing d , shown in Table I. The additional peaks observed between 23°-33° may be due to As₂O₃ (JCPDS file 77-0049 and 83-1548) depicted in Fig. 1. The lattice constants of the selected tetragonal structure were refined using a standard computer program package POWD [23] and found to be $a=3.9763$ Å, $c=8.6469$ Å, $c/a=2.174$. The crystallite size (P) of the compound, roughly estimated using Scherrer's equation [24], was 45 nm.

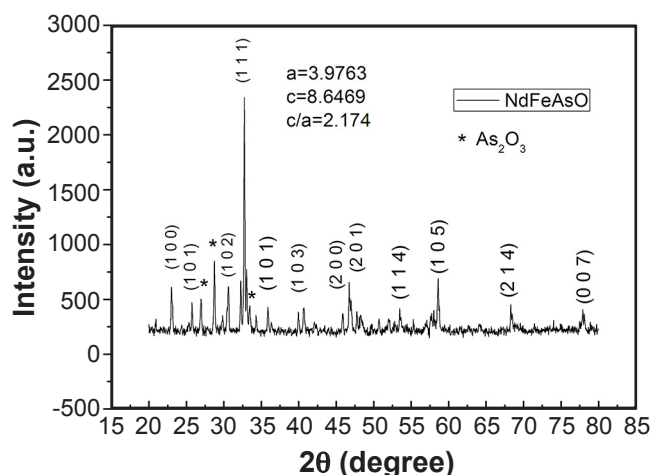


Figure 1: X-ray diffraction pattern of NdFeAsO at room temperature.

Table I - Comparison of observed and calculated d values of NdFeAsO ceramic compound.

hkl	d_{obs} (Å)	d_{cal} (Å)
100	3.8635	3.8763
101	3.4581	3.5126
102	2.9209	2.9267
111	2.6121	2.6239
103	2.2553	2.2337
004	2.2149	2.2017
200	1.9778	1.9881
201	1.9426	1.9376
114	1.7119	1.7138
105	1.5734	1.5859
214	1.3721	1.3733
007	1.2250	1.2353

Dielectric properties: the change of dielectric constant (ϵ_r) and loss tangent ($\tan\delta$) with frequency for NdFeAsO at 25 and 350 °C are given in Fig. 2a and 2b, respectively. It was observed that both the quantities decreased with the increase in frequency, which is typical behavior of most dielectrics samples [25]. The decreasing trend of ϵ_r with the increase in frequency can be attributed to the fact that, at low-frequency range, ϵ_r for polar materials is due to the contribution of all components of polarizability, deformational (electronic, ionic) and relaxational (orientational or dipolar and interfacial or space charge) [26-28]. Hence, higher values of ϵ_r at lower frequencies were mainly due to all types of polarization (i.e., $\alpha_{\text{Total}} = \alpha_{\text{ele}} + \alpha_{\text{ion}} + \alpha_{\text{dip}} + \alpha_{\text{sc}}$, where the subscripts indicate the electronic, ionic, dipolar, and space charge polarization contribution, respectively). In the low-frequency range (10^2 to 10^4 Hz), all types of polarization existed. Since the polarizations are frequency-dependent, some of the polarization dies as the frequency increases and becomes minimum at a higher frequency range. From the variation of ϵ_r with frequency, it is possible to find out the contribution of polarization predominantly present in the sample in a particular frequency range. Further, it was observed that the values of tangent loss at room temperature were found to be of the order of 10^{-1} , which were due to the scattering of charge carriers or defects [29]. The ϵ_r decreased with the increase in frequency up to 10 kHz and became almost constant for the sample, which may be explained by the dipole relaxation process in the compound [30].

The change of ϵ_r with temperature for NdFeAsO in the frequency range of 1 kHz to 4 MHz is depicted in Fig. 3. It was seen that the dielectric constant of the sample increased with the increase in temperature. The increase of ϵ_r value with temperature may be due to the orientational polarization (since it is temperature-dependent). Due to the temperature, the orientation of dipoles is sped up and increases the value of orientational polarization, and hence

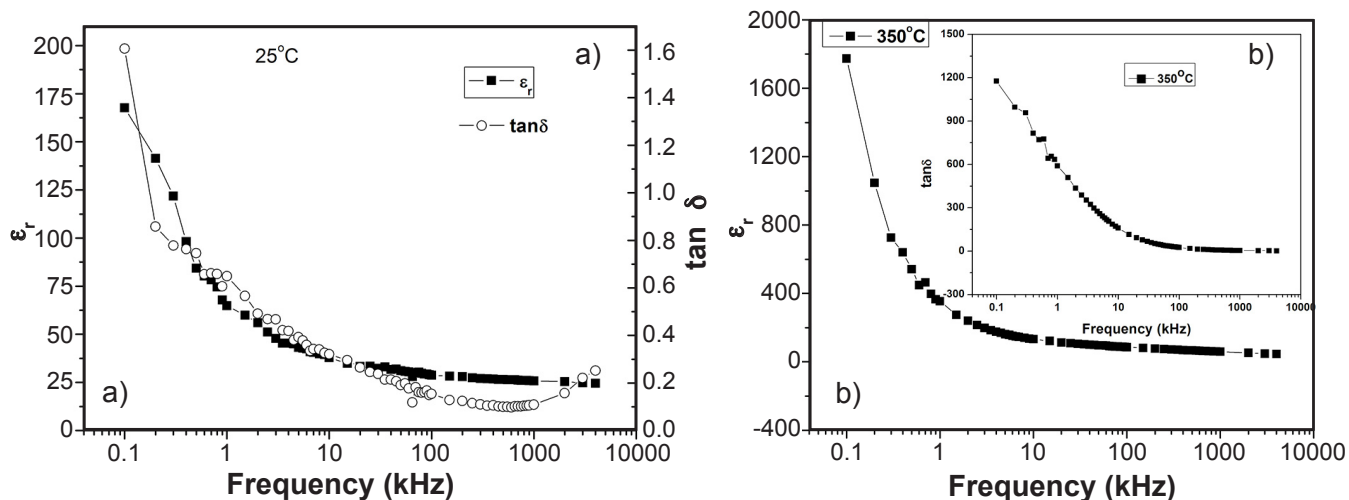


Figure 2: Variation of ϵ_r and $\tan\delta$ of NdFeAsO as a function of frequency at: a) room temperature (25 °C); and b) 350 °C.

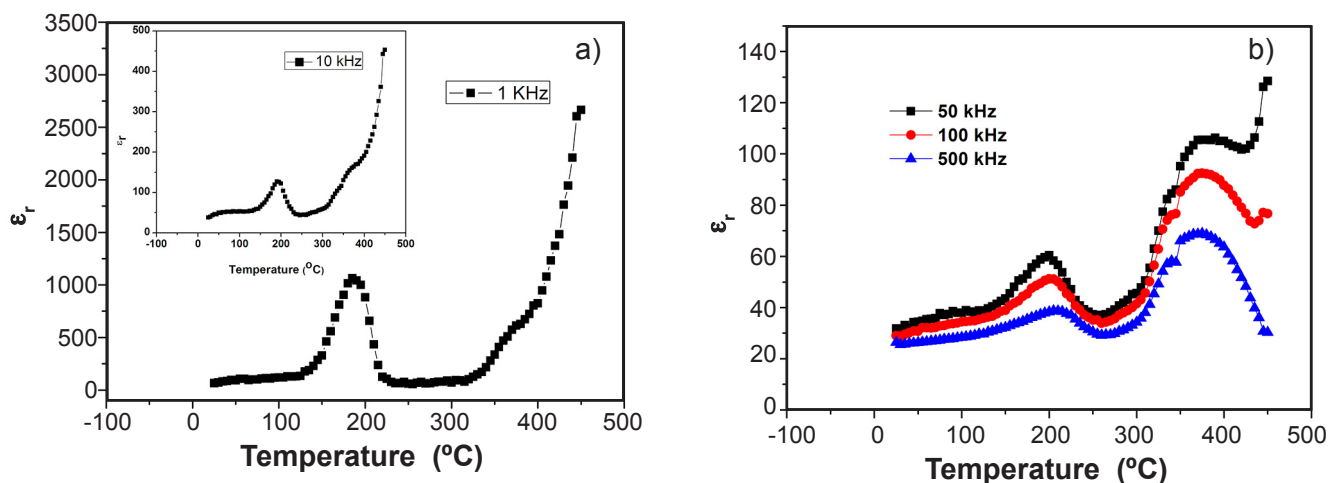


Figure 3: Variation of dielectric constant (ϵ_r) with temperature for NdFeAsO at: a) 1 and 10 kHz; and b) 50, 100, and 500 kHz.

Table II - Comparison of dielectric constant at room temperature and transition temperatures for different frequencies.

Frequency	1 st anomaly (°C)	2 nd anomaly (°C)	ϵ_r at room temperature	ϵ_r at 1 st anomaly	ϵ_r at 2 nd anomaly
1 kHz	185	-	65.10	1062.55	-
10 kHz	190	-	37.30	127.03	-
50 kHz	200	390	31.77	60.44	106.27
100 kHz	200	375	29.05	51.19	92.45
500 kHz	205	375	26.46	38.72	68.92
1 MHz	210	365	25.85	35.33	60.17
2 MHz	215	360	25.38	32.08	52.35
3 MHz	210	350	24.75	30.20	48.28
4 MHz	215	350	24.55	29.26	46.39

the value of dielectric constant [26, 31]. In Fig. 3a, it is observed that an anomaly existed in the dielectric constant at around 185 and 190 °C at 1 and 10 kHz, respectively. In the high-frequency range, there were two anomalies observed. The first anomaly in between 200-215 °C and the second

anomaly in between 350-390 °C were observed. It was also seen that the first dielectric anomaly shifted towards higher temperature sides and the second dielectric anomaly shifted towards the lower temperature side with the increase in frequency. The first dielectric anomaly between 200-215

°C may be due to dipolar relaxation in the materials since the dipolar polarization is temperature dependent and the second anomaly may be due to Maxwell-Wagner relaxation. Both the relaxations may be induced by the hopping motion of the confined carriers as explained below in the density of states section. The values of the dielectric constant at room temperature and the transition temperatures with different frequencies are shown in Table II.

In Fig. 4, the variations of $\tan\delta$ with temperature for NdFeAsO for 1 kHz to 4 MHz are shown. It was observed that the tangent loss of the sample increased with the increase in temperature. The value of $\tan\delta$, which was very small in the low-temperature region, increased sharply with the rise in temperature, which may be due to charge carriers gaining much energy at high temperatures. As a result, the conduction electrons increased with temperature due to thermal activation [32], and hence, $\tan\delta$ increased.

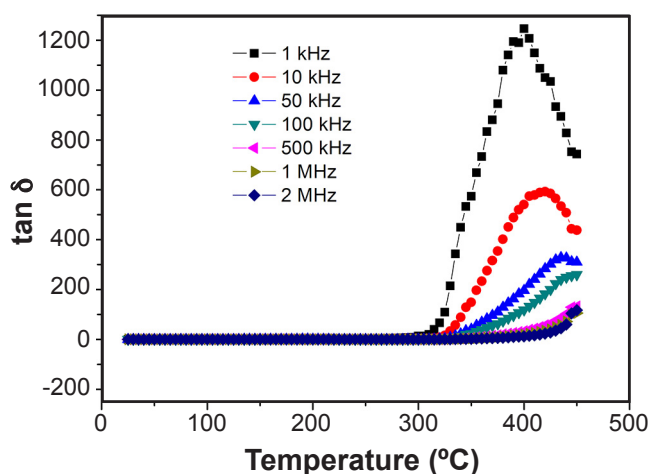


Figure 4: Variation of tangent loss with temperature for NdFeAsO at different frequencies.

AC conductivity analysis: the ac electrical conductivity (σ_{ac}) of the compound was calculated by using an empirical relation $\sigma_{ac} = \omega \cdot \epsilon_r \cdot \epsilon_0 \cdot \tan\delta$, where the symbols have their usual meanings. This helped to explain the nature of the charge carrier and conduction mechanism in the compound. The change in ac conductivity with frequency at various temperatures for NdFeAsO is shown in Fig. 5. It was found that the σ_{ac} increased with the increase in frequency and temperature. At high temperatures, the conductivity spectrum showed a frequency-independent plateau region in the low-frequency range. At high frequencies, there was a tendency to merge the conductivity spectrum and thus the spectrum became temperature and frequency independent. Also at high temperatures, the conductivity spectra showed frequency independent and frequency-dependent regions. Hence, there was a change in the slope of the plots with the increase in temperature as well as frequency. The switch over from the frequency-independent to the frequency-dependent region showed the onset of the conductivity relaxation phenomena and translation from long-range hopping to short-range ionic motion [33, 34]. There was a displacement of the

charge carrier that occurred within the sample by discrete hops of length R between randomly distributed localized sites.

The behavior of conductivity spectra at high temperature followed the universal Jonscher's power law [35] $\sigma(\omega) = \sigma_{dc} + A \cdot \omega^n$, where σ_{dc} is dc conductivity, n is the exponent with $0 < n < 1$, and A is the temperature-dependent pre-exponential factor. The term $A \cdot \omega^n$ explains the dispersion mechanism in the conductivity of the compound by analyzing the values of n. For $n < 1$, the charge carriers are assumed to be taking a translational motion with sudden hopping [36], whereas $n > 1$ would mean a localized hopping of the species with a small hopping without leaving the neighborhood [37]. The value of fitted parameters A and n were calculated from the non-linear fit of the Jonscher's power law given in Table III. The red solid lines in Fig. 5 are the fitted lines. There was a decreasing trend of n with the rise in temperature. This behavior of decreasing trend of n with temperature suggested the conduction mechanism in the compound may be due to the correlated hopping of electrons over a barrier. Hence, the transport mechanism in the compound can be explained by the thermally activated hopping process between two sites separated by an energy barrier. The mechanism for carrier conduction in the sample through the barrier separating the localized sites may be explained by the correlated barrier hopping (CBH) model [38].

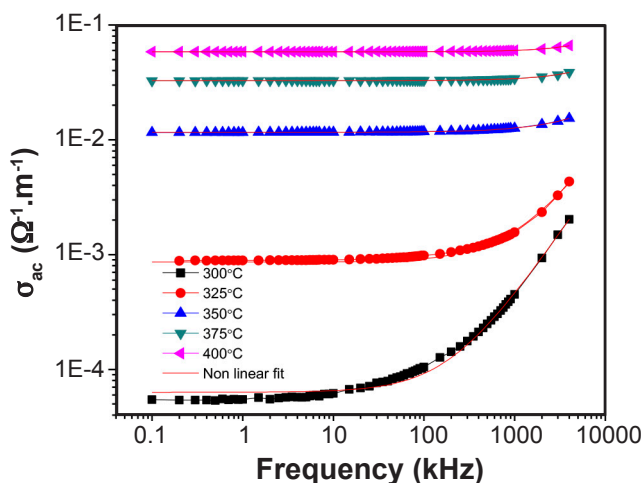


Figure 5: Variation of ac conductivity with the frequency of NdFeAsO in the temperature range of 300 to 400 °C.

Table III - Fitting parameters A and n of the NdFeAsO obtained from Jonscher's power law at different temperatures.

T (°C)	A	n
300	5.44×10^{-11}	0.98
325	2.70×10^{-5}	0.95
350	2.95×10^{-9}	0.90
375	5.47×10^{-10}	0.89
400	1.76×10^{-10}	0.87

Density of states: there are various models proposed to explain the behavior of the conduction mechanism in the semiconducting materials [39]. Based on the CBH model the ac conductivity data have been used to evaluate the density of states at Fermi level $N(E_f)$ using the relation [38-40]:

$$\sigma_{ac}(\omega) = \frac{\pi}{3} e^2 \omega k_B T [N(E_f)]^2 \alpha^{-3} \left[\ln \frac{f_0}{\omega} \right]^4 \quad (A)$$

where e is the electronic charge, f_0 is the photon frequency, and α is the localized wave function, assuming $f_0=10^{13}$ Hz, polarizability $\alpha=10^{10}$ m⁻¹ at various operating frequencies and temperatures. The variation of $N(E_f)$ with frequency at different temperatures (300-400 °C) for the NdFeAsO sample is shown in Fig. 6a and the variation of $N(E_f)$ with the temperature at different frequencies (1 kHz-4 MHz) for NdFeAsO is shown in Fig. 6b. It was observed that the values of $N(E_f)$ decreased with the increase in the frequency and merged at a higher frequency range. Also, it was seen

that the $N(E_f)$ increased with the increase in temperature. At low frequency, the electrical conduction in the system was affected by both the frequency as well as temperature, whereas at higher frequencies the charge carriers were localized and affected by thermal excitations. There was an increase in the density of states with temperature and the reasonably high values of $N(E_f)$ suggested the hopping between the pairs of sites dominated the mechanism of charge transport in the sample [41, 42]. The minimum hopping length, R_{min} was evaluated using the relation:

$$R_{min} = \frac{2e^2}{\pi \epsilon \epsilon_0 W_m} \quad (B)$$

where $W_m=6k_B T/(1-n)$ is the bonding energy. Fig. 7a shows the variation of R_{min} with frequency at different temperatures for NdFeAsO and Fig. 7b shows the variation of R_{min} with the temperature at different frequencies. It was observed that the values of R_{min} increased with the increase in frequency

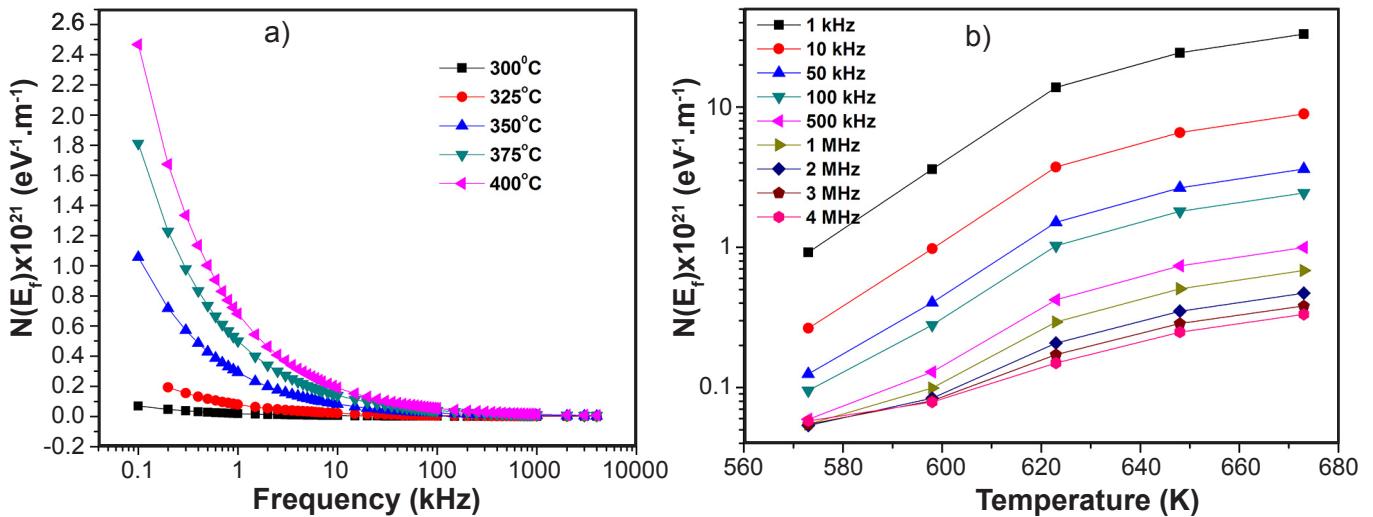


Figure 6: Variation of the density of states $[N(E_f)]$ of NdFeAsO with: a) frequency at different temperatures; and b) temperature at different frequencies.

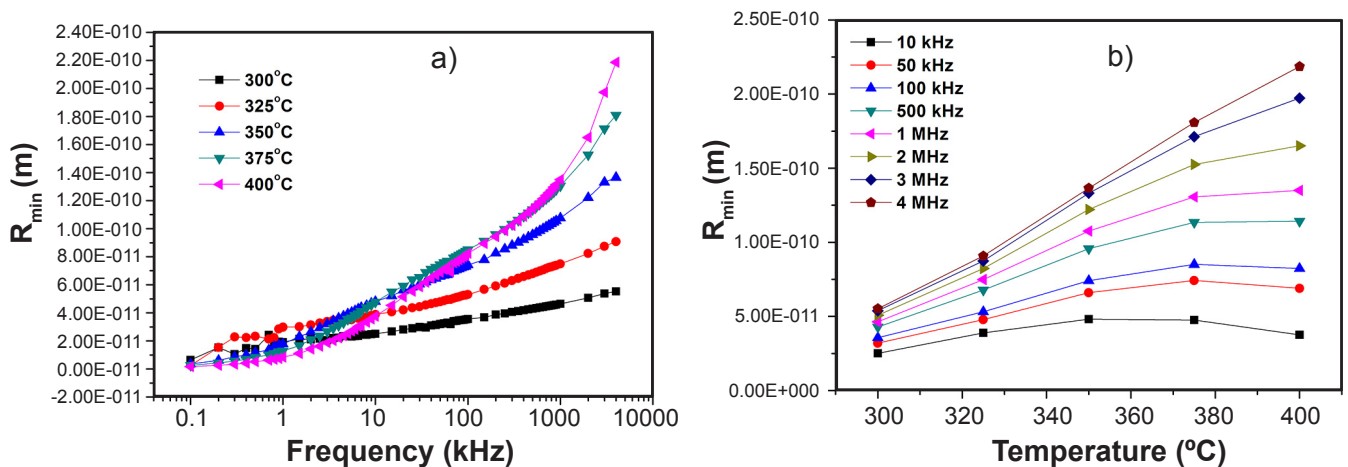


Figure 7: Variation of hopping length (R_{min}) of NdFeAsO with: a) frequency at different temperatures; and b) temperature at different frequencies.

as well as temperature. A very low value ($\sim 10^{-11}$ m) of R_{\min} at the low-frequency region suggested a lack of restoring force involving the mobility of charge carriers under the action of the induced electric field. The R_{\min} increased by sigmoidal nature with the increase in frequency and approaching to a constant value, which suggested the conduction phenomena due to short-range mobility of charge carrier.

The variation of σ_{ac} with the inverse of absolute temperature at different frequencies of NdFeAsO is shown in Fig. 8. The nature of the plot obeying Arrhenius equation is given by:

$$\sigma_{ac} = \sigma_0 \exp\left(\frac{-E_a}{K_B \cdot T}\right) \quad (c)$$

where the symbols have their usual meaning. It was observed that the conductivity increased with the increase in temperature, which showed a negative temperature of coefficient of resistance (NTCR behavior). This was due to the fact that when the temperature increases, the electrons get excited and overcome the barrier that lowers the resistivity. The activation energy calculated from the slope of the plot was in the range between 0.034-0.038 eV with standard errors of 0.01964-0.01968 eV.

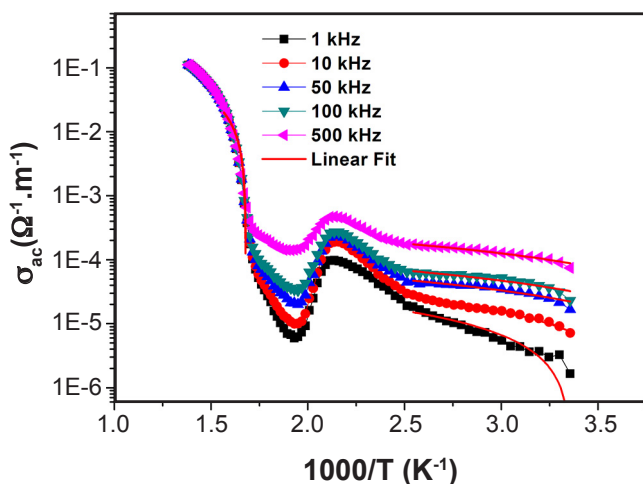


Figure 8: Variation of σ_{ac} with the inverse of absolute temperature at different frequencies for NdFeAsO.

CONCLUSIONS

The solid-state reaction method proved to be a novel way to prepare the proposed sample NdFeAsO. The sample showed a tetragonal structure at room temperature. The crystal size was roughly estimated as 45 nm. The normal behavior of dielectric materials was shown in the sample by showing a similar trend in the change of dielectric constant and tangent loss with frequency and temperature. There were two dielectric anomalies observed in the sample at temperature ranges of 200-215 and 350-390 °C. Due to its dielectric behavior and high dielectric constant, this kind

of iron-based material may be used in capacitor device applications even if its superconducting nature disappears at high temperatures. The universal Jonscher's power law obeyed the ac conductivity spectrum. The sample showed a thermally activated conduction process. The activation energy was found to be in the range of 0.034-0.038 eV. The correlated barrier hopping (CBH) model was successfully used to incorporate the electrical conduction mechanism of the sample.

REFERENCES

- [1] H.A. Boorse, D.B. Cook, M.W. Zemansky, Phys. Rev. **78** (1950) 635.
- [2] C.W. Chu, L. Gao, F. Chen, Z.J. Huang, R.L. Meng, Y.Y. Xue, Nature **365** (1993) 323.
- [3] Y. Kamihara, T. Watanabe, M. Hirano, H. Hosono, J. Am. Chem. Soc. **130** (2008) 3296.
- [4] O. Prakash, A. Kumar, A. Thamizhavel, S. Ramakrishnan, Science **355** (2017) 52.
- [5] Y. Cao, V. Fatemi, S. Fang, K. Watanabe, T. Taniduchi, E. Kaxiras, P.J. Herrero, Nature **556** (2018) 43.
- [6] A.P. Drozdov, M.I. Erements, I.A. Troyan, V. Ksenofontov, S.I. Shylin, Nature **525** (2015) 73.
- [7] Y. Kamihara, H. Hiramatsu, M. Hirano, R. Kawamura, H. Yanagi, T. Kamiya, H. Hosono, J. Am. Chem. Soc. **128** (2006) 10012.
- [8] Y. Kamihara, M. Watanabe, H. Hosono, J. Am. Chem. Soc. **130** (2008) 3296.
- [9] J.H. Tapp, Z. Tang, B. Lv, K. Sasmal, B. Lorenz, P.C.W. Chu, A.M. Guloy, Phys. Rev. B **78** (2008) 60505(R).
- [10] M. Calamiotou, D. Lampakis, N.D. Zhigadlo, S. Katrych, J. Karpinski, A. Fitch, P. Tsiaklagkanos, E. Liarokapis, Physica C Supercond. **527** (2016) 55.
- [11] H. Ota, K. Kudo, T. Kimura, Y. Kitahama, T. Mizukami, S. Ioka, M. Nohara, J. Phys. Soc. Japan **86** (2017) 25002.
- [12] J.G. Bednorz, K.A. Muller, Z. Phys. B Condens. Matter **64** (1986) 189.
- [13] S. Gholipour, V. Daadmehr, A. Rezakhani, H. Khosroabadi, T.F. Shahbaz, R.H. Akbarnejad, J. Supercond. Nov. Magn. **25** (2012) 2253.
- [14] H. Hosono, K. Kuroki, Physica C Supercond. **514** (2015) 399.
- [15] N.L. Wang, H. Hosono, P. Dai (Eds.), "Iron-based superconductors: materials, properties and mechanisms", Taylor Francis (2013) 23.
- [16] S.J. Singh, J. Prakash, S. Patnaik, A.K. Ganguli, Physica C Supercond. **470** (2010) 1928.
- [17] S.J. Cao Wang, Q. Tao, Z. Ren, Y. Li, L. Li, C. Feng, J. Dai, G. Cao, Z. Xu, EPL **86** (2009) 47002.
- [18] Y. Jia, P. Cheng, L. Fang, H. Luo, H. Yang, C. Ren, L. Shan, C. Gu, H.H. Wen, Appl. Phys. Lett. **93** (2008) 32503.
- [19] A. Pattanaik, N.K. Mohanty, P. Nayak, Int. J. Mater. Sci. **5** (2010) 705.
- [20] P.M. Aswathy, J.B. Anooja, N. Varghese, U. Syamaprasad, AIP Conf. Proc. **1665** (2015) 130047.
- [21] A.R. West, Solid state chemistry and its applications,

Wiley (2014)

- [22] H. Kito, H. Eisaki, A. Iyo, J. Phys. Soc. Japan **77** (2008) 63707.
- [23] E. Wu, J. Appl. Cryst. **22** (1989) 506.
- [24] P. Scherrer, Nachr. Akad. Wiss. Gött. **2** (1918) 98.
- [25] J.C. Anderson, *Dielectric*, Chapman Hall, London (1964).
- [26] E. Abd, E.L Wahabb, Acta Phys. Pol. **108** (2005) 6.
- [27] C.J.F. Bottchar, *Theory of electronic polarization*, Elsevier, Amsterdam (1952).
- [28] N.K. Mohanty, A.K Behera, S.K Satpathy, B. Banarji, P. Nayak, J. Rare Earths **33** (2015) 639.
- [29] I.S. Zheludev, *Physics of crystalline dielectrics*, 2, Plenum Press, New York (1971) 455.
- [30] K. Singh, N.S. Negi, R.K. Kotnala, M. Singh, Solid State Commun. **148** (2008) 18.
- [31] B. Tarrev, *Physics of dielectric materials*, Mir Publ., Moscow (1979).
- [32] P.Q. Mantus, J. Eur. Ceram. Soc. **19** (1999) 2079.
- [33] R. Mizaras, M. Takashige, J. Banys, S. Kojima, J. Grigas, S.I. Hamazaki, A. Brilingas, J. Phys. Soc. Japan **66** (1997) 2881.
- [34] K.S. Rao, P.M. Krishna, D.M. Prasad, J.H. Lee, J.S. Kim, J. Alloys Compd. **464** (2008) 497.
- [35] A.K. Jonscher, Nature **267** (1977) 673.
- [36] K. Funke, Prog. Solid State Chem. **22** (1993) 111.
- [37] S. Sen, R.N.P. Choudhary, Mater. Chem. Phys. **87** (2004) 256.
- [38] I.G. Austin, N.F. Mott, Adv. Phys. **18** (1969) 41.
- [39] N.F. Mott, E.A. Davis, *Electronic processes in non-crystalline materials*, 2nd ed., Oxford Un. Press (1979).
- [40] G.D. Sharma, M. Roy, M.S. Roy, Mater. Sci. Eng. B **104** (2003) 15.
- [41] N.K. Mohanty, A.K. Behera, S.K. Satpathy, B. Banarji, P. Nayak, Adv. Mater. Lett. **6** (2015) 947.
- [42] S. Bhagat, K. Prasad, Phys. Status Solidi A **207** (2010) 1232.

(Rec. 14/04/2021, Rev. 16/09/2021, Ac. 20/11/2021)

